INTERNATIONAL JOURNAL FOR NUMERICAL METHODS IN FLUIDS
Int. J. Numer. Meth. Fluids 2011; **00**:1–12
Published online in Wiley InterScience (www.interscience.wiley.com). DOI: 10.1002/fld

Slope limiting for discontinuous Galerkin approximations with a possibly non-orthogonal Taylor basis

D. Kuzmin

Applied Mathematics III, University Erlangen-Nuremberg, Haberstr. 2, D-91058, Erlangen, Germany.

SUMMARY

The use of high-order polynomials in discontinuous Galerkin (DG) approximations to convection-dominated transport problems tends to cause a violation of the maximum principle in regions where the derivatives of the solution are large. In this paper, we express the DG solution in terms of Taylor basis functions associated with the cell average and derivatives at the center of the cell. To control the (derivatives of the) discontinuous solution, the values at the vertices of each element are required to be bounded by the means. This constraint is enforced using a hierarchical vertex-based slope limiter to constrain the coefficients of the Taylor polynomial in a conservative manner starting with the highest-order terms. The loss of accuracy at smooth extrema is avoided by taking the maximum of the correction factors for derivatives of order p and higher. No free parameters, oscillation detectors, or troubled cell markers are involved. In the case of a non-orthogonal Taylor basis, the same limiter is applied to the vector of discretized time derivatives before the multiplication by the off-diagonal part of the consistent mass matrix. This strategy leads to a remarkable gain of accuracy, especially in the case of simplex meshes. A numerical study is performed for a 2D convection equation discretized with linear and quadratic finite elements. Copyright © 2011 John Wiley & Sons, Ltd.

Received . . .

KEY WORDS: convection-dominated transport; finite elements; discontinuous Galerkin methods; hierarchical basis functions non-diagonal mass matrix; slope limiting

1. INTRODUCTION

A major bottleneck in the design of high-order discontinuous Galerkin (DG) methods [5, 6, 8, 11] for convection-dominated transport problems is the lack of reliable mechanisms that ensure nonlinear stability and prevent the onset of spurious oscillations. A variety of discontinuity capturing and slope limiting techniques are available for DG finite element approximations [3, 4, 7, 12, 13, 14, 23] and their finite difference/volume counterparts [2, 21, 25]. However, no universally applicable methodology has been developed to date. Since the accuracy of monotonicity-preserving schemes degenerates to first order at local extrema, free parameters or heuristic indicators are frequently employed to distinguish between the troubled cells and regions where the solution varies smoothly. In our experience, the reliability of many oscillation detectors leaves a lot to be desired.

The parameter-free slope limiter proposed in [15] is based on a geometric maximum principle for the DG solution and its derivatives. As shown by Aizinger [1], it can be interpreted as a local optimization problem. The use of Taylor basis functions [20, 21, 25] makes it possible to adjust the derivatives without changing the mean values. In the case of a piecewise-linear DG approximation, the algorithm differs from the Barth-Jespersen limiter [2] merely in the definition of the upper and lower bounds for the solution values at the vertices of the mesh. The gradient and space derivatives of higher order (if any) are limited in the same manner. Since derivatives of order p possess higher regularity than those of order $q > p$, they are limited by at most the same amount. The hierarchical approach to slope limiting preserves smooth peaks without resorting to troubled cell markers.

The vertex-based limiter produces the best results if the Taylor basis is orthogonal. The orthogonality condition holds for a uniform mesh of rectangular elements but not for triangles, tetrahedra or general quadrilaterals/hexahedra. Nonzero off-diagonal entries of the mass matrix give rise to an implicit coupling between the (unconstrained) derivatives of all orders. The application of the slope limiter to the resultant solution yields non-oscillatory but distorted approximations, which explains the relatively poor performance of the limiter in the numerical study by Michoski et al. [22]. In the original work [15], we performed all computations using the diagonal part of the mass matrix for the Taylor basis. This mass lumping strategy is conservative but also results in a loss of accuracy in the case of strongly time-dependent problems. In particular, the potential benefits of higher-order finite elements (including the preservation of smooth extrema) may be lost. Our conclusion was: "the inclusion of a non-diagonal mass matrix would require the implementation of a limiter for the involved *time* derivatives" [15]. This conjecture turned out to be true.

In this article, we apply the vertex-based slope limiter to the vector of discretized time derivatives calculated using the full mass matrix. The corrected contribution of its off-diagonal part is added to the right-hand side of the lumped-mass discretization. This compensates the mass lumping error in regions where the time derivative varies smoothly in space. We used a similar approach to constrain the consistent mass matrix for continuous (linear and multilinear) finite elements in [16]. The results to be presented indicate that the time-limited DG approximation on a triangular mesh is even more accurate than that on a quadrilateral mesh with the same vertices and an orthogonal Taylor basis.

2. UPWIND DG FORMULATION

A simple model problem that will serve as a vehicle for the presentation of the improved slope limiter for high-order DG approximations is the linear convection equation

$$\frac{\partial u}{\partial t} + \nabla \cdot (\mathbf{v}u) = 0 \qquad \text{in } \Omega, \tag{1}$$

where $u(\mathbf{x},t)$ is a scalar quantity transported by a continuous velocity field $\mathbf{v}(\mathbf{x},t)$. Let $\mathbf{n}$ denote the unit outward normal to the boundary Γ of Ω. The initial and boundary conditions are given by

$$u|_{t=0} = u_0, \qquad u|_{\Gamma_{\text{in}}} = g, \qquad \Gamma_{\text{in}} = \{\mathbf{x} \in \Gamma \,|\, \mathbf{v}\cdot\mathbf{n} < 0\}.$$

Multiplying (1) by a sufficiently smooth test function w, integrating over Ω, and using Green's formula, one obtains the following weak formulation

$$\int_\Omega \left(w\frac{\partial u}{\partial t} - \nabla w \cdot \mathbf{v}u \right) \mathrm{d}\mathbf{x} + \int_\Gamma wu\mathbf{v}\cdot\mathbf{n}\,\mathrm{d}s = 0, \qquad \forall w. \tag{2}$$

In the DG method, the domain Ω is decomposed into a finite number of cells Ω_e, and a local polynomial basis $\{\varphi_j\}$ is employed to define the approximate solution

$$u_h(\mathbf{x},t)|_{\Omega_e} = \sum_j u_j(t)\varphi_j(\mathbf{x}), \qquad \forall \mathbf{x} \in \Omega_e. \tag{3}$$

The globally defined function $u_h : \Omega \times [0,T] \mapsto \mathbb{R}$ is piecewise-polynomial and may have jumps at interelement boundaries. A local version of problem (2) can be formulated as

$$\int_{\Omega_e} \left(w_h\frac{\partial u_h}{\partial t} - \nabla w_h \cdot \mathbf{v}u_h \right) \mathrm{d}\mathbf{x} + \int_{\Gamma_e} w_h\hat{u}_h\mathbf{v}\cdot\mathbf{n}\,\mathrm{d}s = 0, \qquad \forall w_h, \tag{4}$$

where $w_h \in \{\varphi_i\}$ is a test function from the DG space. Since u_h is multiply defined on Γ_e, the surface integral is calculated using the solution value from the upwind side of the interface, i.e.,

$$\hat{u}_h(\mathbf{x},t)|_{\Gamma_e} = \begin{cases} \lim\limits_{\delta\to+0} u_h(\mathbf{x}+\delta\mathbf{n},t), & \mathbf{v}\cdot\mathbf{n} < 0, \quad \mathbf{x} \in \bar{\Omega}\backslash\Gamma_{\text{in}}, \\ g(\mathbf{x},t), & \mathbf{v}\cdot\mathbf{n} < 0, \quad \mathbf{x} \in \Gamma_{\text{in}}, \\ \lim\limits_{\delta\to+0} u_h(\mathbf{x}-\delta\mathbf{n},t), & \mathbf{v}\cdot\mathbf{n} \geq 0, \quad \mathbf{x} \in \bar{\Omega}. \end{cases} \tag{5}$$

DOI: 10.1002/fld

In the case of a piecewise-constant approximation, one obtains the first-order accurate upwind finite volume scheme. The DG formulation for general conservation laws is described, e.g., in [6, 7, 11].

3. TAYLOR BASIS FUNCTIONS

In a discontinuous Galerkin method of degree $p \geq 0$, the shape function $u_h|_{\Omega_e}$ is given by (3), where the number of basis functions depends on p. Following Luo *et al.* [20], we restrict our discussion to quadratic polynomials $u_h|_{\Omega_e} \in P_2(\Omega_e)$ and consider the 2D Taylor series expansion

$$\begin{aligned} u_h(x,y) = u_c + \tfrac{\partial u}{\partial x}\big|_c (x-x_c) + \tfrac{\partial u}{\partial y}\Big|_c (y-y_c) + \tfrac{\partial^2 u}{\partial x^2}\Big|_c \tfrac{(x-x_c)^2}{2} \\ + \tfrac{\partial^2 u}{\partial y^2}\Big|_c \tfrac{(y-y_c)^2}{2} + \tfrac{\partial^2 u}{\partial x \partial y}\Big|_c (x-x_c)(y-y_c) \end{aligned} \tag{6}$$

about the centroid (x_c, y_c) of a cell Ω_e. Introducing the volume averages

$$\bar{u}_h = \frac{1}{|\Omega_e|}\int_{\Omega_e} u_h \,\mathrm{d}\mathbf{x}, \qquad \overline{x^n y^m} = \frac{1}{|\Omega_e|}\int_{\Omega_e} x^n y^m \,\mathrm{d}\mathbf{x},$$

the quadratic function u_h can be expressed in the equivalent form [20, 21, 25]

$$\begin{aligned} u_h(x,y) = \bar{u}_h + \tfrac{\partial u}{\partial x}\big|_c (x-x_c) + \tfrac{\partial u}{\partial y}\Big|_c (y-y_c) \\ + \tfrac{\partial^2 u}{\partial x^2}\Big|_c \left[\tfrac{(x-x_c)^2}{2} - \overline{\tfrac{(x-x_c)^2}{2}}\right] + \tfrac{\partial^2 u}{\partial y^2}\Big|_c \left[\tfrac{(y-y_c)^2}{2} - \overline{\tfrac{(y-y_c)^2}{2}}\right] \\ + \tfrac{\partial^2 u}{\partial x \partial y}\Big|_c \left[(x-x_c)(y-y_c) - \overline{(x-x_c)(y-y_c)}\right]. \end{aligned} \tag{7}$$

This representation has led Luo *et al.* [20] to consider the local Taylor basis

$$\begin{aligned} &\varphi_1 = 1, \quad \varphi_2 = \tfrac{x-x_c}{\Delta x}, \quad \varphi_3 = \tfrac{y-y_c}{\Delta y}, \quad \varphi_4 = \tfrac{(x-x_c)^2}{2\Delta x^2} - \overline{\tfrac{(x-x_c)^2}{2\Delta x^2}}, \\ &\varphi_5 = \tfrac{(y-y_c)^2}{2\Delta y^2} - \overline{\tfrac{(y-y_c)^2}{2\Delta y^2}}, \quad \varphi_6 = \tfrac{(x-x_c)(y-y_c) - \overline{(x-x_c)(y-y_c)}}{\Delta x \Delta y}. \end{aligned} \tag{8}$$

The scaling by $\Delta x = (x_{\max} - x_{\min})/2$ and $\Delta y = (y_{\max} - y_{\min})/2$ is required to improve the condition number of the algebraic system [20]. The normalized degrees of freedom are proportional to the cell mean value $\bar{u}_h$ and derivatives of u_h at the point (x_c, y_c). We have

$$\begin{aligned} u_h(x,y) = \bar{u}_h\varphi_1 + \left(\tfrac{\partial u}{\partial x}\big|_c \Delta x\right)\varphi_2 + \left(\tfrac{\partial u}{\partial y}\Big|_c \Delta y\right)\varphi_3 + \left(\tfrac{\partial^2 u}{\partial x^2}\Big|_c \Delta x^2\right)\varphi_4 \\ + \left(\tfrac{\partial^2 u}{\partial y^2}\Big|_c \Delta y^2\right)\varphi_5 + \left(\tfrac{\partial^2 u}{\partial x \partial y}\Big|_c \Delta x \Delta y\right)\varphi_6. \end{aligned} \tag{9}$$

Note that the cell averages are decoupled from other degrees of freedom since

$$\int_{\Omega_e} \varphi_1^2 \,\mathrm{d}\mathbf{x} = |\Omega_e|, \qquad \int_{\Omega_e} \varphi_1 \varphi_j \,\mathrm{d}\mathbf{x} = 0, \qquad 2 \leq j \leq 6.$$

On a uniform mesh of rectangular elements, the Taylor basis (8) is orthogonal [7]. On a triangular mesh, this is not the case even for the linear part $\{\varphi_1, \varphi_2, \varphi_3\}$ since the L_2 inner product of φ_2 and φ_3 is nonzero. A non-diagonal mass matrix M may be 'lumped' by setting all off-diagonal entries equal to zero. In contrast to the case of a typical Lagrange basis, this modification is conservative since it does not affect the decoupled equation for the mean value of u_h in Ω_e. However, mass lumping degrades the phase accuracy and should be avoided whenever possible (see below).

DOI: 10.1002/fld

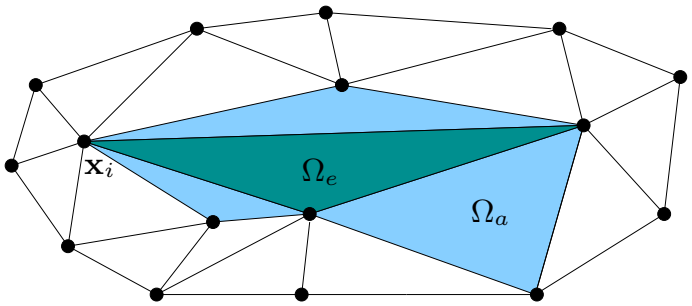

Figure 1. Vertices and neighbors of Ω_e on a triangular mesh.

4. THE VERTEX-BASED LIMITER

The above Taylor series representation is amenable to p-adaptation and limiting. In the context of finite volume and DG finite element methods, a slope limiter is typically implemented as a postprocessing filter that constrains a polynomial shape function to stay within certain bounds. Many unstructured grid codes are equipped with the limiter developed by Barth and Jespersen [2] for piecewise-linear approximations. Given a cell average $\bar{u}_h = u_c$ and the gradient $(\nabla u)_c$, the objective is to determine the steepest admissible slope for a constrained reconstruction of the form

$$u_h(\mathbf{x}) = u_c + \alpha_e (\nabla u)_c \cdot (\mathbf{x} - \mathbf{x}_c), \qquad 0 \le \alpha_e \le 1, \quad \mathbf{x} \in \Omega_e. \tag{10}$$

Barth and Jespersen [2] define the correction factor α_e so that the final solution values at a number of control points $\mathbf{x}_i \in \Gamma_e$ are bounded by the maximum and minimum centroid values found in Ω_e or in one of its neighbors Ω_a having a common edge (in 2D) or face (in 3D) with Ω_e, see Fig. 1

$$u_e^{\min} \le u(\mathbf{x}_i) \le u_e^{\max}, \qquad \forall i. \tag{11}$$

Due to linearity, the solution u_h attains its local extrema at the vertices $\mathbf{x}_i$ of the cell Ω_e. Hence, a vertex-based limiting strategy is appropriate. The above definition of $u_e^{\max}$ and $u_e^{\min}$ implies that

- different bounds are imposed on the solution value at vertex $\mathbf{x}_i$ in different elements;
- $u_e^{\max}$ or $u_e^{\min}$ may be a centroid value in a neighbor element that does not contain $\mathbf{x}_i$;
- no constraints are imposed on the difference between the values of $u(\mathbf{x}_i)$ in neighbor elements that share the vertex $\mathbf{x}_i$ but have no common edge / face;
- the results are rather sensitive to the geometric properties of the mesh.

This has led us to replace the elementwise bounds $u_e^{\max}$ and $u_e^{\min}$ with the maximum and minimum of centroid values in the patch of elements containing $\mathbf{x}_i$. The so-defined $u_i^{\max}$ and $u_i^{\min}$ may be initialized by a small/large constant and updated in a loop over elements Ω_e as follows:

$$u_i^{\max} := \max\{u_c, u_i^{\max}\}, \tag{12}$$

$$u_i^{\min} := \min\{u_c, u_i^{\min}\}. \tag{13}$$

The geometric constraint that dictates the choice of the correction factor α_e for (10) becomes

$$u_i^{\min} \le u(\mathbf{x}_i) \le u_i^{\max}, \qquad \forall i \tag{14}$$

and we enforce it using the simple formula [15]

$$\alpha_e = \min_i \begin{cases} \min\left\{1, \frac{u_i^{\max} - u_c}{u_i - u_c}\right\}, & \text{if } u_i - u_c > 0, \\ 1, & \text{if } u_i - u_c = 0, \\ \min\left\{1, \frac{u_i^{\min} - u_c}{u_i - u_c}\right\}, & \text{if } u_i - u_c < 0, \end{cases} \tag{15}$$

DOI: 10.1002/fld

where u_i denotes the tentative unconstrained solution value at the vertex $\mathbf{x}_i \in \Omega_e$. That is,

$$u_i = u_c + (\nabla u)_c \cdot (\mathbf{x}_i - \mathbf{x}_c).$$

The only difference as compared to the classical Barth-Jespersen (BJ) limiter is the use of $u_i^{\max\min}$ in place of $u_e^{\max\min}$. This seemingly minor modification turns out to be the key to achieving high accuracy with p-adaptive DG methods [15]. In fact, the revised limiting strategy resembles the elementwise version of the finite element flux-corrected transport (FEM-FCT) algorithm developed by Löhner *et al.* [18]. In explicit FCT schemes, $u_i^{\max}$ and $u_i^{\min}$ represent the local extrema of a low-order solution. In accordance with the local discrete maximum principle for unsteady problems, data from the previous time level can also be involved in the estimation of admissible upper/lower bounds.

5. LIMITING HIGHER-ORDER TERMS

The quality of the slope limiting procedure is particularly important in the case of a high-order DG method [13]. Poor accuracy and/or lack of robustness restrict the practical utility of many parameter-dependent algorithms and heuristic generalizations of limiters developed for piecewise-linear functions. Following Yang and Wang [25], we multiply all derivatives of order p by a common correction factor $\alpha_e^{(p)}$. The limited counterpart of the Taylor series expansion (7) becomes

$$\begin{aligned} u_h(x,y) = \bar{u}_h &+ \alpha_e^{(1)} \left\{ \tfrac{\partial u}{\partial x}\Big|_c (x-x_c) + \tfrac{\partial u}{\partial y}\Big|_c (y-y_c) \right\} \\ &+ \alpha_e^{(2)} \left\{ \tfrac{\partial^2 u}{\partial x^2}\Big|_c \left[\tfrac{(x-x_c)^2}{2} - \overline{\tfrac{(x-x_c)^2}{2}} \right] + \tfrac{\partial^2 u}{\partial y^2}\Big|_c \left[\tfrac{(y-y_c)^2}{2} - \overline{\tfrac{(y-y_c)^2}{2}} \right] \right. \\ &\left. + \tfrac{\partial^2 u}{\partial x \partial y}\Big|_c \left[(x-x_c)(y-y_c) - \overline{(x-x_c)(y-y_c)} \right] \right\}. \end{aligned} \tag{16}$$

The so-defined u_h is a quadratic polynomial, so its first derivatives are linear, and their gradients are given by the constant second-order derivatives. Hence, the gradients can be limited in the same fashion as cell averages. In our method [15], the values of the correction factors $\alpha_e^{(1)}$ and $\alpha_e^{(2)}$ are determined using the vertex-based limiter as applied to the linear reconstructions

$$u_x^{(2)}(x,y) = \frac{\partial u}{\partial x}\Big|_c + \alpha_x^{(2)} \left\{ \frac{\partial^2 u}{\partial x^2}\Big|_c (x-x_c) + \frac{\partial^2 u}{\partial x \partial y}\Big|_c (y-y_c) \right\}, \tag{17}$$

$$u_y^{(2)}(x,y) = \frac{\partial u}{\partial y}\Big|_c + \alpha_y^{(2)} \left\{ \frac{\partial^2 u}{\partial x \partial y}\Big|_c (x-x_c) + \frac{\partial^2 u}{\partial y^2}\Big|_c (y-y_c) \right\}, \tag{18}$$

$$u^{(1)}(x,y) = \bar{u}_h + \alpha_e^{(1)} \left\{ \frac{\partial u}{\partial x}\Big|_c (x-x_c) + \frac{\partial u}{\partial y}\Big|_c (y-y_c) \right\}. \tag{19}$$

Since the mixed second derivative appears in (17) and (18), the correction factor $\alpha_e^{(2)}$ for all second-order terms in the limited P_2 approximation (16) is defined by

$$\alpha_e^{(2)} = \min\{\alpha_x^{(2)}, \alpha_y^{(2)}\}. \tag{20}$$

The first derivatives of the DG solution are typically smoother and should be multiplied by

$$\alpha_e^{(1)} := \max\{\alpha_e^{(1)}, \alpha_e^{(2)}\} \tag{21}$$

to avoid the loss of accuracy at smooth extrema. It is important to implement the limiter as a hierarchical p-coarsening algorithm, as opposed to making the assumption [7] that no oscillations are present in u_h if they are not detected in the linear part. In general, we begin with the highest-order derivatives (cf. [13, 25]) and calculate a nondecreasing sequence of correction factors

$$\alpha_e^{(p)} := \max_{p \le q} \alpha_e^{(q)}, \qquad p \ge 1. \tag{22}$$

Prepared using fldauth.cls
DOI: 10.1002/fld

As soon as $\alpha_e^{(q)} = 1$ is encountered, no further limiting is required since definition (22) implies that $\alpha_e^{(p)} = 1$ for all $p \le q$. Remarkably, there is no penalty for using the maximum correction factor. At least for scalar equations, discontinuities are resolved in a sharp and nonoscillatory manner [15].

6. LIMITING THE TIME DERIVATIVES

The semi-discrete DG scheme can be written as a system of differential-algebraic equations

$$M_C \frac{\mathrm{d}u}{\mathrm{d}t} = r(u), \tag{23}$$

where $u = \{u_j\}$ is the vector of unknowns, $M_C = \{m_{ij}\}$ is the (block-diagonal) mass matrix, and $r(u)$ is the discretized convective term, including fluxes across the inflow boundary.

The oscillatory modes of the DG solution are filtered out in the process of slope limiting. The solution vector u and the vector $\frac{\mathrm{d}u}{\mathrm{d}t}$ are constrained independently using the algorithm presented in Sections 4 and 5. The bounds for the time derivatives at the vertices are defined in terms of the cell-centered time derivatives. In practice, the limiter is applied after the discretization in time.

The time integration method for the semi-discrete problem (23) should guarantee nonlinear stability, at least for sufficiently small time steps Δt. Gottlieb and Shu [9] introduced a family of explicit Runge-Kutta methods that preserve the *total variation diminishing* (TVD) property of a 1D space discretization. In general, such time-stepping schemes can be classified as *strong stability-preserving* (SSP) [10]. If the forward Euler method is SSP, so are its high-order counterparts, perhaps under a different restriction on the time step. For details, we refer to the review paper by Gottlieb *et al.* [10]. In this article, we use the optimal third-order SSP Runge-Kutta scheme [9]

$$u^{(1)} = u^n + \Delta t M_C^{-1} r(u^n), \tag{24}$$

$$u^{(2)} = \frac{3}{4}u^n + \frac{1}{4}\left[u^{(1)} + \Delta t M_C^{-1} r(u^{(1)})\right], \tag{25}$$

$$u^{n+1} = \frac{1}{3}u^n + \frac{2}{3}\left[u^{(2)} + \Delta t M_C^{-1} r(u^{(2)})\right]. \tag{26}$$

Since the DG mass matrix M_C is block-diagonal, it can be inverted efficiently element-by-element.

In the slope-limited version of the above RKDG method, we update the solution as follows:

1. Given $u^{(k-1)}$, calculate the vector of discretized time derivatives given by
$$\dot{u}^{(k)} = M_C^{-1} r(u^{(k-1)}). \tag{27}$$
2. Apply the hierarchical vertex limiter Φ to the predictor $\dot{u}^{(k)}$ and calculate
$$\tilde{u}^{(k)} = u^{(k-1)} + \Delta t M_L^{-1}[(M_L - M_C)\Phi\dot{u}^{(k)} + r(u^{(k-1)})], \tag{28}$$
where $M_L := \mathrm{diag}\{m_{ii}\}$ denotes the diagonal part of the mass matrix M_C.
3. Apply the hierarchical vertex limiter Φ to the convex average of u^n and $\tilde{u}^{(k)}$
$$u^{(k)} = \Phi(\omega_k u^n + (1-\omega_k)\tilde{u}^{(k)}), \tag{29}$$
where $\omega_k \in [0,1]$ is the weight for step k of the SSP Runge-Kutta scheme.

The first step should be omitted if the Taylor basis is orthogonal ($M_L = M_C$). If no limiting is performed in the second step ($\Phi\dot{u} = \dot{u}$), the result is the consistent-mass DG approximation

$$\tilde{u}^{(k)} = u^{(k-1)} + \Delta t M_C^{-1} r(u^{(k-1)}). \tag{30}$$

The application of the slope limiter to $\dot{u}^{(k)}$ eliminates the contribution of non-smooth spatial variations in the time derivatives of u_h, which improves the phase characteristics of the constrained DG scheme. In the case of a non-orthogonal Taylor basis, this sort of time limiting is a must for the reasons explained in the Introduction. The extra cost is justified by a marked gain of accuracy.

A time-stepping scheme like (24)–(26) may serve as a smoother for a fast p-multigrid solver [19] in which only coarse-level approximations are treated implicitly for efficiency reasons.

DOI: 10.1002/fld

7. A NUMERICAL STUDY

The solid body rotation test proposed by LeVeque [17] is a standard 2D benchmark for numerical advection schemes. The problem to be solved is (1) with the incompressible velocity field

$$\mathbf{v}(x,y) = (0.5 - y, x - 0.5) \tag{31}$$

that describes a counterclockwise rotation about the center of $\Omega := (0,1) \times (0,1)$. After each full revolution, the exact solution u coincides with the initial data u_0. Hence, this test is designed to evaluate the ability of a numerical scheme to preserve the shape of the solution profile.

Following LeVeque [17], we simulate solid body rotation of a slotted cylinder, a sharp cone, and a smooth hump (see Fig. 2a). The geometry of each body is described by a function $G(x,y)$ defined on a circle of radius $r_0 = 0.15$ centered at a certain point (x_0, y_0). Let

$$r(x,y) = \frac{1}{r_0}\sqrt{(x-x_0)^2 + (y-y_0)^2}$$

be the normalized distance from the point (x_0, y_0). Then $r(x,y) \le 1$ inside the circle.

The slotted cylinder is centered at the point $(x_0, y_0) = (0.5, 0.75)$ and

$$G(x,y) = \begin{cases} 1 & \text{if } |x - x_0| \ge 0.025 \ \text{ or } \ y \ge 0.85, \\ 0 & \text{otherwise.} \end{cases}$$

The cone is centered at $(x_0, y_0) = (0.5, 0.25)$, and its shape is given by

$$G(x,y) = 1 - r(x,y).$$

The hump is centered at $(x_0, y_0) = (0.25, 0.5)$, and the shape function is

$$G(x,y) = \frac{1 + \cos(\pi r(x,y))}{4}.$$

Of course, not only cell averages but also the derivatives of the solution must be initialized properly.

In this section, we solve the above test problem using DG approximations with orthogonal and non-orthogonal Taylor bases. The errors $E_2 = ||u - u_h||_2$ are measured in the L_2 norm at the final time $t = 2\pi$. For visualization purposes, the approximate solution u_h is L_2-projected into the space V_h of continuous piecewise-linear or bilinear functions using the formula

$$\int_\Omega \tilde{w}_h \tilde{u}_h \, \mathrm{d}\mathbf{x} = \sum_e \int_{\Omega_e} \tilde{w}_h u_h \, \mathrm{d}\mathbf{x}, \qquad \forall \tilde{w}_h \in V_h.$$

Mass lumping is employed in the current implementation of this postprocessing step which has a smoothing effect. The limiter does a nice job if at least $\tilde{u}_h$ is free of undershoots and overshoots.

The numerical solutions presented in Fig. 2 were calculated with the RKDG method on a uniform mesh of rectangular elements. The mesh size and time step for this simulation are given by $h = 1/128$ and $\Delta t = 10^{-3}$, respectively. The DG-P_0 approximation produces the diffusive solution shown in Fig. 2b. The limited DG-P_1 approximation is more accurate but exhibits peak clipping (Fig. 2c), whereas the DG-P_2 version (Fig. 2d) preserves the two peaks remarkably well.

The results for the limited P_1 and P_2 approximations on a triangular mesh with the same vertices are displayed in Fig. 3. In this case, the Taylor basis (8) is non-orthogonal, which means that there are implicit links between the derivatives of the DG solution in each element. The computation of $\tilde{u}^{(k)}$ using (29) without limiting produces the inaccurate solutions shown in Fig. 3a–b. Replacing the full mass matrix M_C with its diagonal part M_L, one obtains the results in Fig. 3c–d. Note that the P_2 solution is just marginally better than its P_1 counterpart and also exhibits peak clipping. The last diagrams (Fig. 3e-f) were calculated with algorithm (27)–(28). The application of the vertex-based limiter to the vector of time derivatives makes it possible to recover the high accuracy of the P_2 approximation in smooth regions, and the results are even better than those in Fig. 2c–d.

DOI: 10.1002/fld

(a) Initial/exact solution, $E_2 = 0.0$

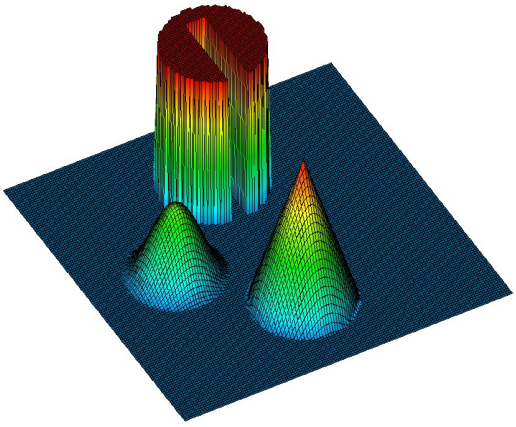

(b) P_0 elements, E_2=1.80e-1

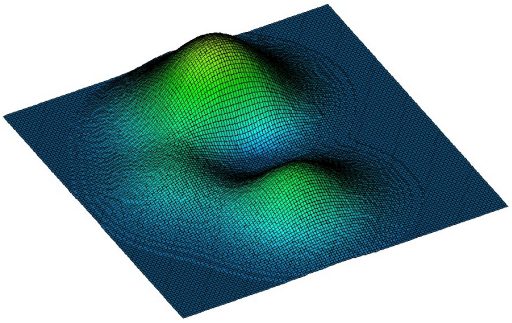

(c) P_1 elements, E_2=7.19e-2

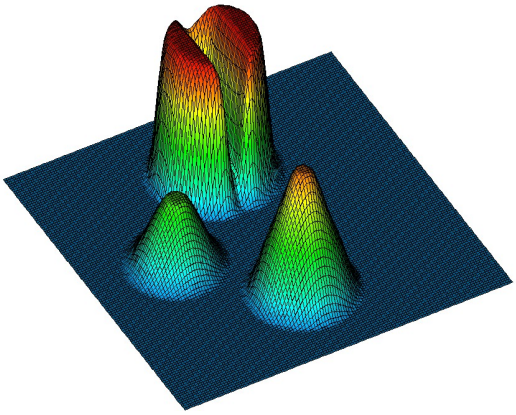

(d) P_2 elements, E_2=6.60e-2

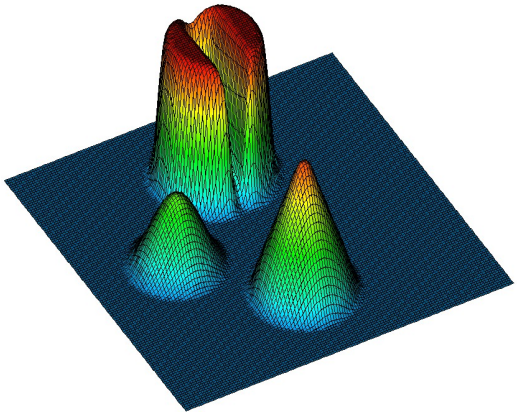

Figure 2. Solid body rotation, simulation on a rectangular mesh, $t = 2\pi$.

For a better visual comparison of the solution profiles, we present 4 cutlines of the initial and final DG solutions in Figs 4–6. The difference between the P_1 and P_2 approximations is particularly pronounced near the two peaks. Note that the P_2 version of the RKDG method resolves the smooth hump ($x = 0.25$) perfectly if the Taylor basis is orthogonal (Fig. 4c) or if the off-diagonal part of the mass matrix is applied to the vector of *limited* time derivatives (Fig. 6c). The peak of the cone ($y = 0.25$) is also preserved much better than in the P_1 version. In the neighborhood of the slotted cylinder ($y = 0.75$), the vertex-based slope limiter switches to the monotone DG-0 approximation. Therefore, the differences between the limited P_1 and P_2 solutions are marginal in this region.

8. CONCLUSIONS

In this paper, we addressed a new aspect of slope limiting for high-order discontinuous Galerkin approximations with a possibly non-orthogonal Taylor basis. The implementation of the presented algorithm in an existing DG code may require an elementwise transformation of basis. For example, Michoski et al. [22] use the Dubiner basis functions to compute the DG solution but perform limiting in terms of the Taylor basis functions. Of course, our methodology is not restricted to the linear convection equation. The vertex-based slope limiter has already been applied to the equations of

DOI: 10.1002/fld

(a) P_1 / consistent mass, E_2=1.33e-1

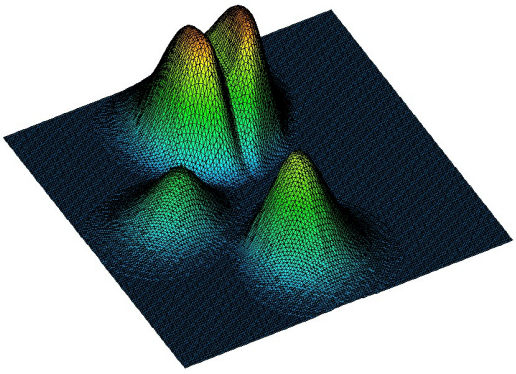

(b) P_2 / consistent mass, E_2=1.11e-1

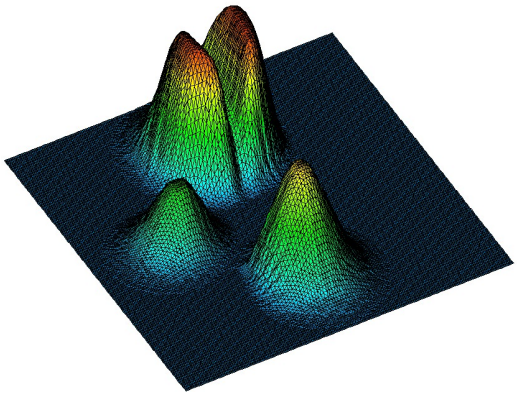

(c) P_1 / lumped mass, E_2=6.81e-2

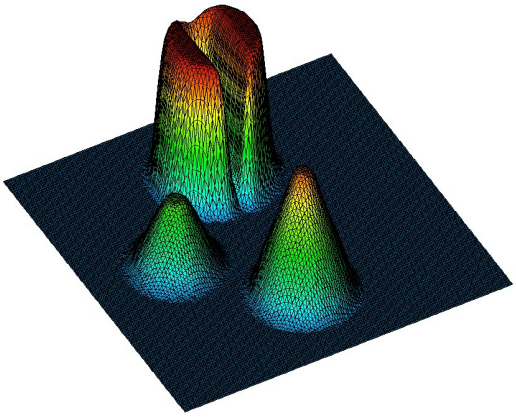

(d) P_2 / lumped mass, E_2=6.70e-2

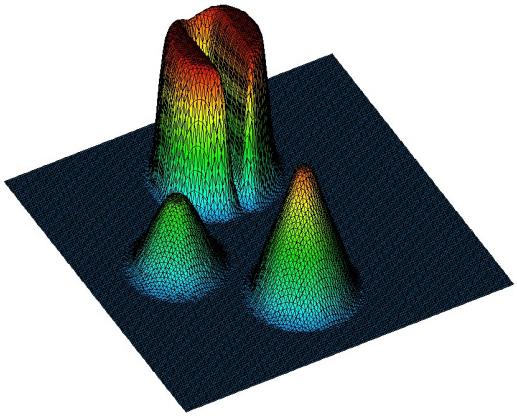

(e) P_1 / limited mass, E_2=6.50e-2

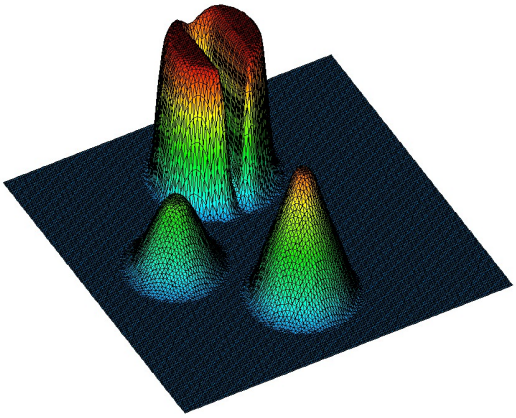

(f) P_2 / limited mass, E_2=6.05e-2

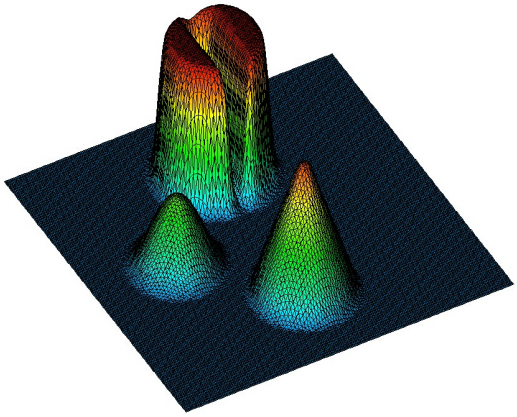

Figure 3. Solid body rotation, simulation on a triangular mesh, $t = 2\pi$.

gas dynamics [24] and to the 3D shallow water equations [1] with considerable success. We also envisage its embedding into hp-FEM and combination with implicit time-stepping schemes.

DOI: 10.1002/fld

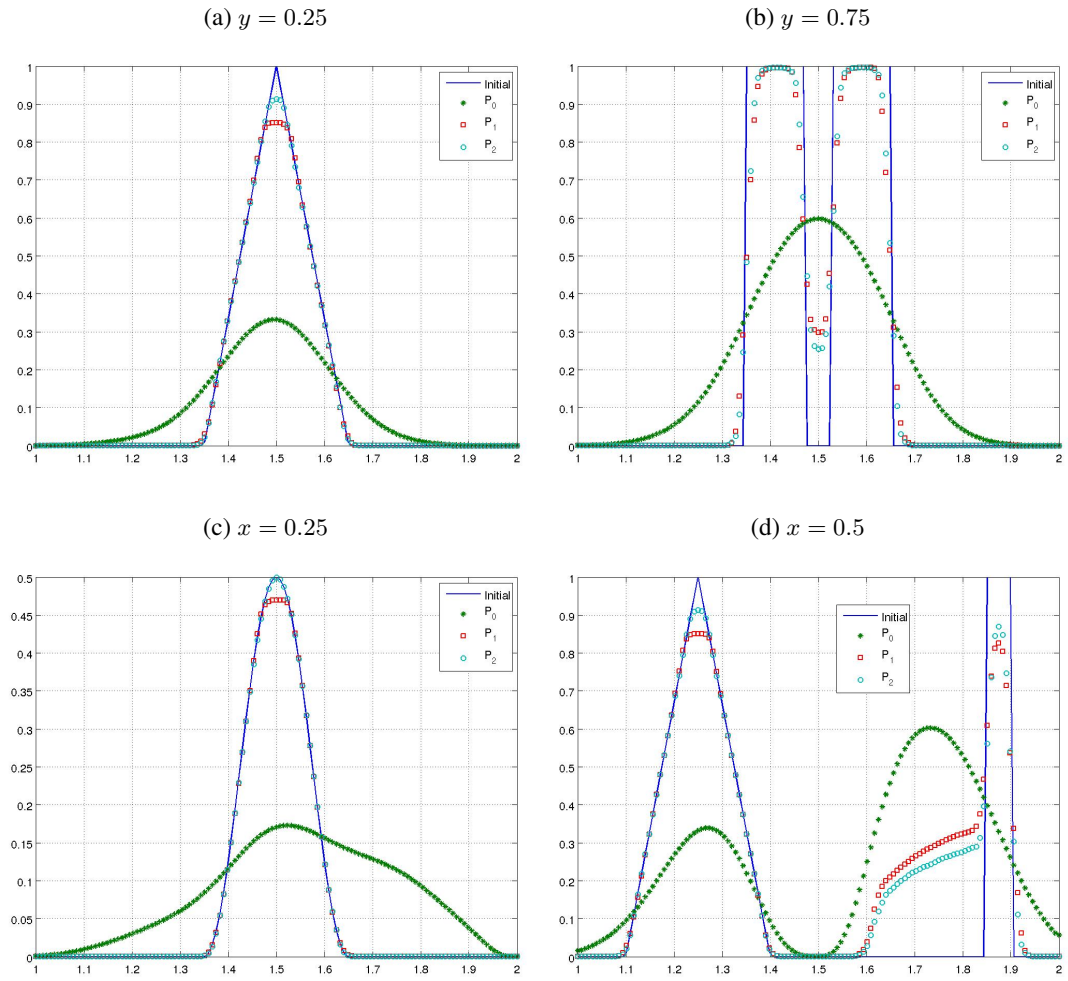

Figure 4. Cutlines of the DG solutions on the rectangular mesh, $t = 2\pi$.

Acknowledgments

This research was supported by the German Research Association (DFG) under grant KU 1530/6-1.

REFERENCES

1. V. Aizinger, A geometry independent slope limiter for the discontinuous Galerkin method. In: *Notes on Numerical Fluid Mechanics and Multidisciplinary Design*, Volume 115 (2011) 207-217.
2. T. Barth and D.C. Jespersen, The design and application of upwind schemes on unstructured meshes. *AIAA Paper*, 89-0366, 1989.
3. R. Biswas, K. Devine, and J. E. Flaherty, Parallel adaptive finite element methods for conservation laws. *Appl. Numer. Math.* **14** (1994) 255–284.
4. A. Burbeau, P. Sagaut, and C.-H. Bruneau, A problem-independent limiter for high-order Runge-Kutta discontinuous Galerkin methods. *J. Comput. Phys.* **169** (2001) 111–150.
5. B. Cockburn, G.E. Karniadakis, and C.-W. Shu, The development of discontinuous Galerkin methods. In: B. Cockburn, G.E. Karniadakis, and C.-W. Shu (eds), *Discontinuous Galerkin Methods. Theory, Computation and Applications*, LNCSE **11** (2000), Springer, New York, 3–50.
6. B. Cockburn and C.-W. Shu, Runge-Kutta discontinuous Galerkin methods for convection-dominated problems. *J. Sci. Comput.* **16** (2001) 173–261.
7. B. Cockburn and C.-W. Shu, The Runge-Kutta discontinuous Galerkin method for conservation laws V. Multidimensional Systems. *J. Comput. Phys.* **141** (1998) 199–224.

DOI: 10.1002/fld

(a) $y = 0.25$ (b) $y = 0.75$

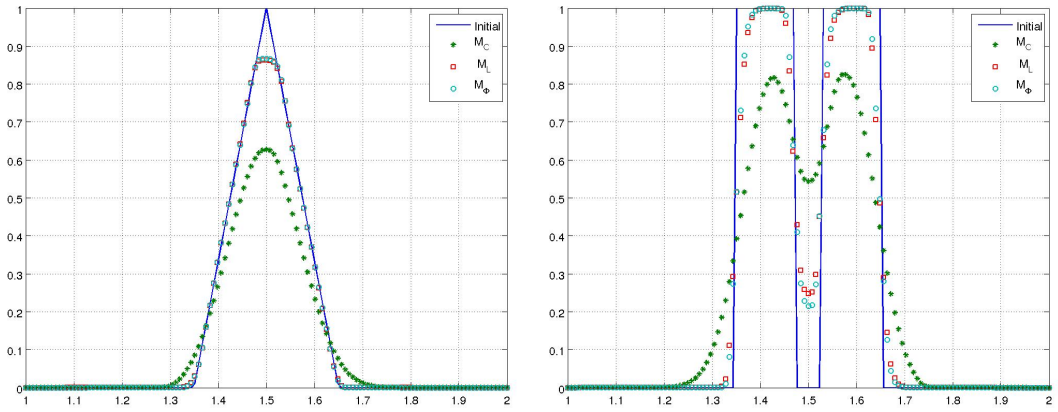

(c) $x = 0.25$ (d) $x = 0.5$

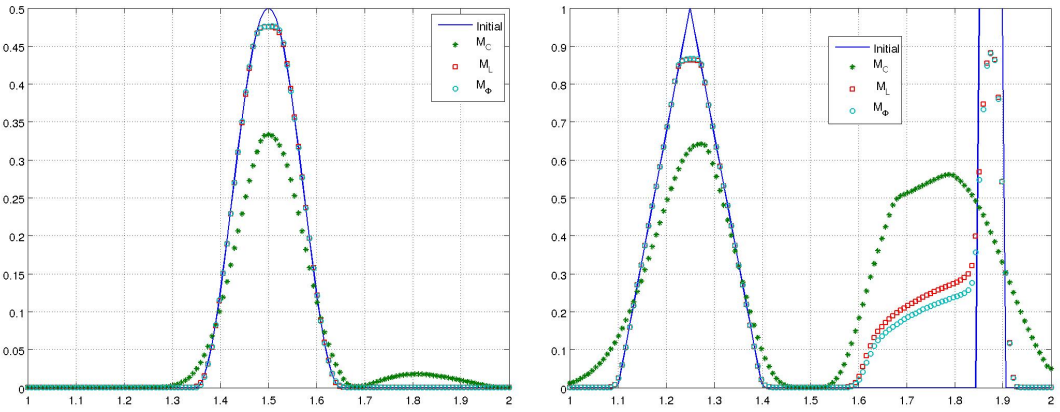

Figure 5. Cutlines of the P_1 solutions on the rectangular mesh, $t = 2\pi$.

8. J.E. Flaherty, L. Krivodonova, J.-F. Remacle, and M.S. Shephard, Aspects of discontinuous Galerkin methods for hyperbolic conservation laws. *Finite Elements in Analysis and Design* **38** (2002) 889–908.
9. S. Gottlieb and C.-W. Shu, Total Variation Diminishing Runge-Kutta schemes. *Math. Comp.* **67** (1998) 73–85.
10. S. Gottlieb, C.-W. Shu, and E. Tadmor, Strong stability-preserving high-order time discretization methods. *SIAM Review* **43** (2001) 89–112.
11. J.S. Hesthaven and T. Warburton, *Nodal Discontinuous Galerkin Methods: Algorithms, Analysis, and Applications.* Springer Texts in Applied Mathematics **54**, Springer, New York, 2008.
12. H. Hoteit, Ph. Ackerer, R. Mosé, J. Erhel, and B. Philippe, New two-dimensional slope limiters for discontinuous Galerkin methods on arbitrary meshes. *Int. J. Numer. Meth. Engrg.* **61** (2004) 2566–2593.
13. L. Krivodonova, Limiters for high-order discontinuous Galerkin methods. *J. Comput. Phys.* **226** (2007) 879–896.
14. L. Krivodonova, J. Xin, J.-F. Remacle, N. Chevaugeon, and J.E. Flaherty, Shock detection and limiting with discontinuous Galerkin methods for hyperbolic conservation laws. *Appl. Numer. Math.* **48** (2004) 323–338.
15. D. Kuzmin, A vertex-based hierarchical slope limiter for p-adaptive discontinuous Galerkin methods. *J. Comput. Appl. Math.* **233** (2010) 3077–3085.
16. D. Kuzmin, Linearity-preserving flux correction and convergence acceleration for constrained Galerkin schemes. *Ergebnisberichte Angew. Math.* **421**, TU Dortmund, 2011. Submitted to *J. Comput. Appl. Math.*
17. R.J. LeVeque, High-resolution conservative algorithms for advection in incompressible flow. *SIAM J. Numer. Anal.* **33** (1996) 627–665.
18. R. Löhner, K. Morgan, J. Peraire, and M. Vahdati, Finite element flux-corrected transport (FEM-FCT) for the Euler and Navier-Stokes equations. *Int. J. Numer. Meth. Fluids* **7** (1987) 1093–1109.
19. H. Luo, J.D. Baum, and R. Löhner, Fast p-multigrid discontinuous Galerkin method for compressible flows at all speeds. *AIAA Journal* **46** (2008) 635–652.
20. H. Luo, J.D. Baum, and R. Löhner, A discontinuous Galerkin method based on a Taylor basis for the compressible flows on arbitrary grids. *J. Comput. Phys.* **227** (2008) 8875–8893.

DOI: 10.1002/fld

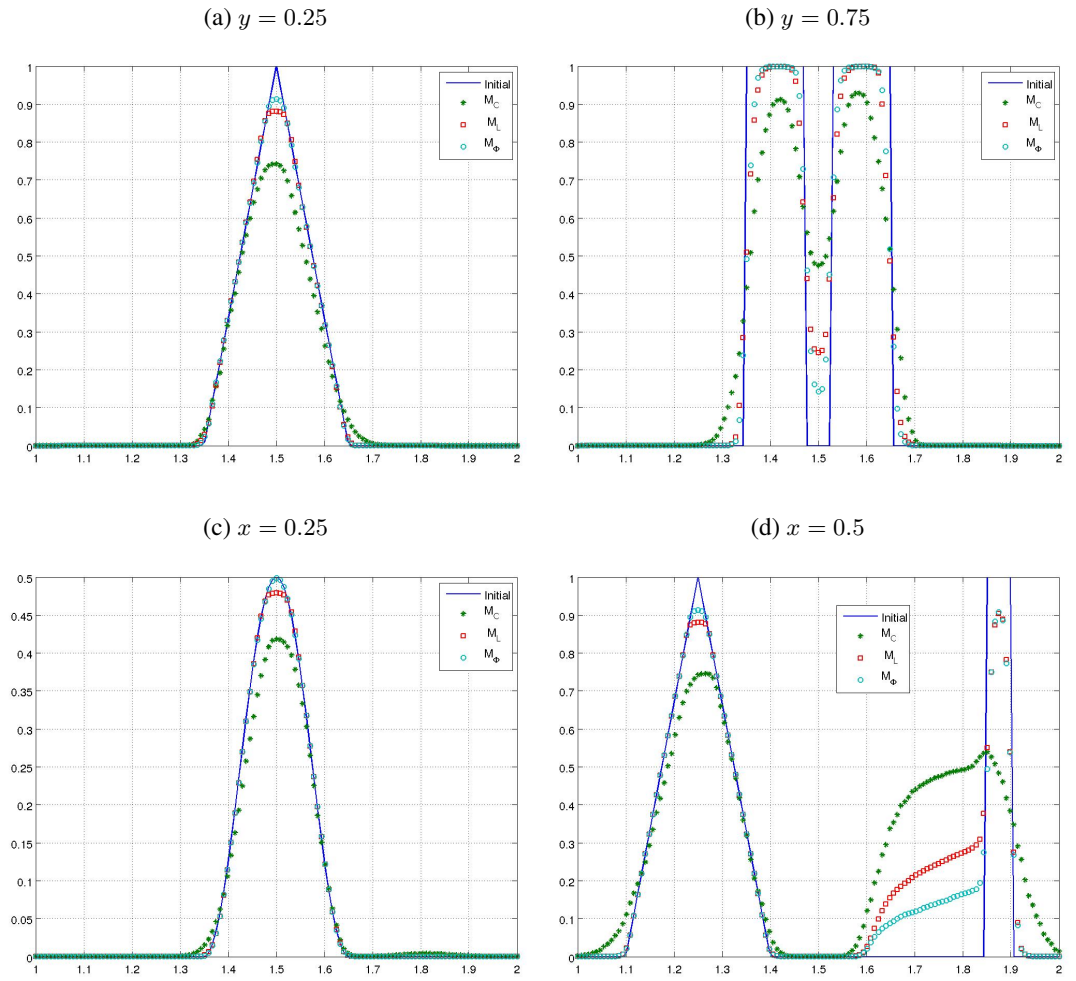

Figure 6. Cutlines of the P_2 solutions on the triangular mesh, $t = 2\pi$.

21. K. Michalak and C. Ollivier-Gooch, Limiters for unstructured higher-order accurate solutions of the Euler equations. In: Proceedings of the *AIAA Forty-Sixth Aerospace Sciences Meeting*, 2008.
22. C. Michoski, C. Mirabito, C. Dawson, E.J Kubatko, D. Wirasaet, and J.J. Westerink, Adaptive hierarchic transformations for dynamically p-enriched slope-limiting over discontinuous Galerkin systems of generalized equations. Submitted to *J. Comput. Phys.* (2010).
23. S. Tu and S. Aliabadi, A slope limiting procedure in discontinuous Galerkin finite element method for gasdynamics applications. *Int. J. Numer. Anal. Model.* **2** (2005) 163–178.
24. F. Vilar, P.H. Maire and R. Abgrall, Cell-centered discontinuous Galerkin discretizations for two-dimensional scalar conservation laws on unstructured grids and for one-dimensional Lagrangian hydrodynamics. *Computers & Fluids* **46** (2011) 498–504.
25. M. Yang and Z.J. Wang, A parameter-free generalized moment limiter for high-order methods on unstructured grids, AIAA-2009-605.

DOI: 10.1002/fld